ACS APPLIED NANO MATERIALS

Open Access

This article is licensed under CC-BY 4.0

www.acsanm.org

Article

Visible-Light-Driven Porphyrin/ZnO Nanohybrids for Ultrasensitive Room-Temperature Triethylamine Sensing

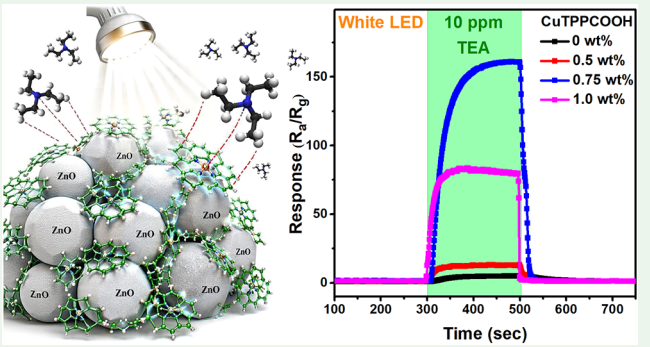
Van Duy Lai, Thi Nguyet To, Valerio Allegra, Roberto Paolesse, Gabriele Magna, Franco Biasioli, Matteo Tonezzer,* Alexandro Catini, and Corrado Di Natale*

Cite This: *ACS Appl. Nano Mater.* 2026, 9, 16061−16074

Read Online

ACCESS | Metrics & More | Article Recommendations | Supporting Information

ABSTRACT: Real-time monitoring of toxic triethylamine (TEA) at room temperature remains a significant challenge for metal oxide chemiresistors due to their typically high-power consumption and thermal requirements. This work presents a highly responsive, visible-light-activated gas sensor based on ZnO nanoparticles (25.5 nm crystallites) functionalized with Cu-porphyrin (CuTPP-COOH). By leveraging the visible-light-harvesting properties of the porphyrin integrated into a nanoscale organic/inorganic heterojunction, the hybrid sensor operates efficiently at room temperature, completely eliminating the need for thermal heating. Owing to the nanoscale dimensions of the oxide domains, which maximize boundary depletion region modulation, the optimized device exhibits an ultralow theoretical limit of detection of 0.4 ppb and a superior response (162 toward 10 ppm TEA), significantly outperforming pristine ZnO nanostructures and current state-of-the-art sensors. The sensing enhancement is driven by a synergistic photoinduced charge transfer at the functionalized nanometer-scale interface, which maximizes sensing response under visible light illumination. With demonstrated high selectivity, excellent moisture stability, and rapid response dynamics, this nanoengineered hybrid architecture offers a robust, low-power solution for next-generation environmental safety networks and portable TEA monitors.

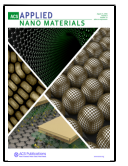


KEYWORDS: *gas sensor, ZnO nanoparticles, porphyrin, hybrid sensor, triethylamine, light activation*

1. INTRODUCTION

The detection of hazardous gases is critical for ensuring environmental quality and human health.[1] Triethylamine (TEA), a volatile tertiary amine widely employed as a catalyst, corrosion inhibitor, and intermediate in chemical synthesis, poses particular risk owing to its caustic, flammable, and toxic nature.[2] Exposure to TEA can cause respiratory and dermal irritation, as well as systemic toxicity. Accordingly, the American Conference of Governmental Industrial Hygienists (ACGIH) has set threshold limit values at 1 ppm for short-term exposure and 0.5 ppm for time-weighted average exposure,[3] while the National Fire Protection Association (NFPA) assigns TEA a hazard rating of 3 for both health and flammability.[4] Conventional analytical methods such as gas chromatography and mass spectrometry offer high accuracy but require expensive equipment, trained personnel, and long analysis times. By contrast, chemiresistive metal oxide (MOX) gas sensors provide a simple, low-cost, and compact solution for real-time monitoring of toxic gases and volatile organic compounds (VOCs).[5] ZnO, an n-type semiconductor with a wide band gap (3.37 eV) and large exciton binding energy (60 meV), has been extensively investigated as a sensing material owing to its chemical stability, abundance, and tunable surface properties. However, pristine ZnO sensors often require high operating temperatures (>200 °C) and suffer from limited selectivity, restricting their practical use.[6,7] To address these drawbacks, several approaches have been investigated, such as the construction of inorganic p-n heterojunction networks. For instance, CuO/ZnO architectures have demonstrated significant potential in reducing the thermal activation energy and enhancing the room-temperature chemiresistive response toward specific volatile compounds, including ammonia[8] and triethylamine (TEA).[9] Recent strategies to improve room-temperature MOS sensing focus on interfacial engineering and structural design. These include $Ti_3C_2T_x/SnO_2$ heterostructures driven by Schottky barrier modulation,[10] α-Fe_2O_3 nanostructures with engineered faces and enhanced oxygen vacancies,[11] and MOF-derived NiO-SnO_2 composites that exploit p−n junctions for ppb-level sensing.[12] In addition to

Received: June 25, 2026
Revised: August 5, 2026
Accepted: August 6, 2026
Published: August 12, 2026



ACS Publications

© 2026 The Authors. Published by American Chemical Society

Downloaded from pubs.acs.org/aanmf6/article-pdf/9/33/16061/6652975/acsanm.6c02958.pdf by guest on 22 October 2026

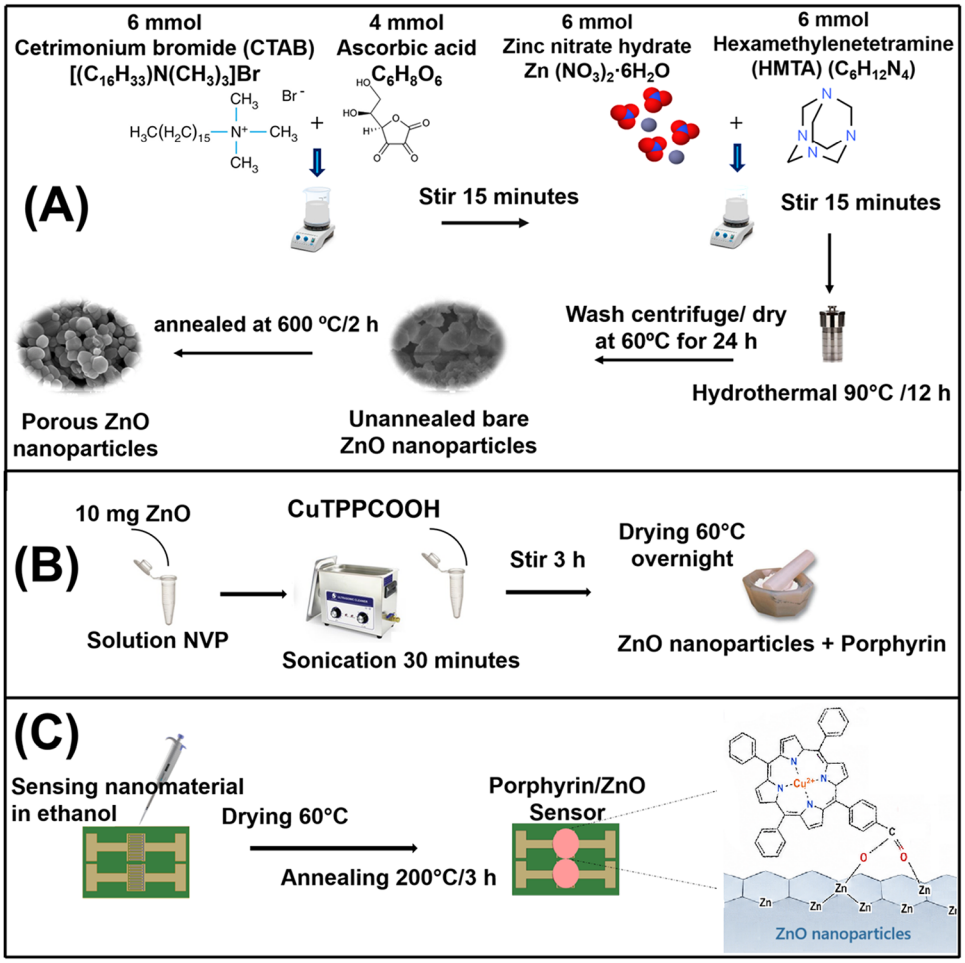


Figure 1. Synthesis of ZnO and Cu-porphyrin/ZnO nanomaterials: (A) synthesis of ZnO nanoparticles; (B) synthesis of nanohybrid material and (C) device fabrication and surface chemical structure.

chemiresistive platforms, FET-based devices using carbon nanotubes and catalytic gates have achieved subppm hydrogen sensing through signal amplification.[13] While these methods highlight the advantages of defect and band engineering, coupling photosensitive organic macrocycles such as porphyrins with ZnO provides a distinct, light-driven alternative for ultrasensitive operation at room temperature without thermal input. Alternatively, surface functionalization is a widely adopted strategy to overcome these limitations. Decorating MOX materials with noble metals (e.g., Pd, Au, Pt)[14] or organic semiconductors (e.g., phthalocyanines, porphyrins, conducting polymers)[15] can reduce the operating temperature, enhance catalytic activity, and improve gas specificity.

Porphyrins, in particular, are attractive modifiers due to their extended π-electron conjugation,[16] versatile functionalization at both central metal and peripheral positions,[17] and strong optical absorption in the visible range.[18] These features enable porphyrins to act as efficient electron donors/acceptors and photosensitizers, thereby enhancing gas adsorption and facilitating charge transfer under light illumination. Copper-porphyrins are especially promising for amine sensing, as the planar conjugated macrocycle provides a robust supramolecular recognition platform for amines via π-stacking interactions, while the square-planar Cu(II) center, which does not participate in axial coordination, remains unaffected, avoiding potential interferences at the metal site. The macrocycle simultaneously mediates photoinduced charge separation, enabling efficient electron transfer upon visible light excitation.[19]

Despite these advancements, a systematic comparison of room-temperature TEA sensors reveals a persistent trade-off between sensitivity, operational stability, and the energy required for activation. While various metal oxide heterojunctions (e.g., CuO/ZnO, NiO/ZnO) have successfully lowered operational temperatures, they often lack the required specificity for trace-level TEA detection in complex environments. Simultaneously, existing porphyrin-based sensitizers frequently face limitations regarding long-term photostability and the efficiency of interfacial charge injection, which often results in sluggish response/recovery kinetics. Consequently, there remains a critical need for a sensing architecture that concurrently leverages high-surface-area nanostructured matrices and molecularly engineered photosensitizers to achieve subppb limits of detection at room temperature. The specific scientific gap addressed herein lies in the design of a controlled organic/inorganic nanoscale heterojunction where the porphyrin moiety acts not merely as a passive receptor, but as an active "light-harvesting antenna" capable of modulating the ZnO depletion layer via photoexcited charge transfer. We hypothesize that the rational alignment of the porphyrin LUMO with the ZnO conduction band over nanoscale interfacial contact areas, combined with the efficient charge

https://doi.org/10.1021/acsanm.6c02958
ACS Appl. Nano Mater. 2026, 9, 16061−16074

Downloaded from pubs.acs.org/aanmf6/article-pdf/9/33/16061/6652075/acsanm.6c02958.pdf by guest on 22 October 2026

separation enabled by the type-II heterojunction, will bypass traditional thermal activation requirements, offering a highly selective and stable solution for reversible and real-time TEA monitoring.

In this study we report the synthesis of hybrid combining sub-30 nm crystalline ZnO primary nanoparticles functionalized with a Cu-porphyrin derivative. The resulting nanostructured sensors demonstrate exceptional sensing performance to TEA vapors at room temperature, surpassing the performance of pure ZnO nanoparticles, particularly under white LED illumination. The optimized sensor containing 0.75 wt % Cu-porphyrin exhibited a response of 162 to 10 ppm TEA under ambient conditions, with a theoretical limit of detection of 0.4 ppb. The hybrid also displayed excellent selectivity against common interferents, reproducibility, and long-term stability over six months. These results highlight the potential of Cu-porphyrin/ZnO nanohybrids as robust, low-power, and highly effective materials for TEA detection in industrial safety, environmental monitoring, and healthcare applications.

2. EXPERIMENTAL SECTION

2.1. Materials Preparation

L-ascorbic acid ($C_6H_8O_6$), hexadecyltrimethylammonium bromide (CTAB, $C_{19}H_{42}BrN$), hexamethylenetetramine (HMTA, $C_6H_{12}N_4$), and zinc nitrate hexahydrate ($Zn(NO_3)_2{\cdot}6H_2O$) were bought from Sigma-Aldrich and used without further purification. 5-(4′-carboxyphenyl)-10,15,20-triphenylporphyrin-copper (CuTPPCOOH) was synthesized according to a previously reported procedure.[20] All aqueous solutions were prepared using deionized water.

2.2. Synthesis of ZnO Nanoparticles

ZnO nanoparticles were synthesized via a CTAB-assisted hydrothermal method (Figure 1A). Initially, 6 mmol of CTAB and 4 mmol of ascorbic acid were dissolved in 60 mL of deionized water under magnetic stirring for 15 min. Then, 6 mmol of zinc nitrate hexahydrate and 6 mmol of HMTA were added, stirring for another 15 min until the mixture reached a pH of 5. The solution was transferred into a 100 mL Teflon-lined stainless-steel autoclave and maintained at 90 °C for 12 h. After natural cooling to room temperature, the precipitate was collected by centrifugation at 4000 rpm for 10 min, washed five times with deionized water and ethanol, and dried in an oven at 60 °C for 24 h. Finally, the dried powder was calcined at 600 °C for 2 h in air (heating rate 2 °C/min) to obtain crystalline ZnO nanoparticles.

2.3. Synthesis of CuTPPCOOH-Coated ZnO Nanoparticles

For surface modification, 10 mg of ZnO NPs were dispersed in 10 mL of N-vinylpyrrolidone under ultrasonication for 30 min to obtain a stable colloidal suspension (Figure 1B). Different amounts of porphyrin (0, 0.5, 0.75, and 1 wt %) were then added to compare the properties of different hybrid nanomaterials. The mixtures were mechanically stirred for 3 h at room temperature to ensure uniform coating, followed by solvent evaporation at 60 °C and drying overnight. The resulting powders were gently ground in an agate mortar before further use.

2.4. Materials Characterization

The morphology of the nanomaterials was investigated by field-emission scanning electron microscopy (FE-SEM, JEOL JSM-7600F). Crystal structure was analyzed by powder X-ray diffraction (XRD, Advance D8, Bruker with Cu−Kα1 radiation, λ = 1.54056 Å). Elemental composition was determined using energy-dispersive X-ray spectroscopy (EDS, attached to the SEM). High-resolution transmission electron microscopy (HRTEM, JEOL, JEM-2100F) was used to observe lattice fringes and particle−porphyrin interfaces. Optical absorption spectra were collected using a UV−Vis spectrophotometer (Cary 100 Conc, Varian). The nature of the bonds in the materials was investigated by Raman spectroscopy obtained with a Renishaw inVia confocal micro-Raman system. Fourier transform infrared (FTIR) spectra were recorded on a FT/IR-4600 type A spectrometer (JASCO, Japan). Nitrogen adsorption−desorption isotherms were acquired using a Micromeritics Gemini VII analyzer, and surface area and pore size distribution were calculated by the BET and BJH methods, respectively.

2.5. Sensor Fabrication and Gas-Sensing Measurements

The ZnO and CuTPPCOOH/ZnO powders were dispersed in ethanol (10 mg/mL) and drop-cast onto interdigitated Pt electrodes (gap 100 μm, electrode area 5 mm × 5 mm) to create thick film sensors (Figure 1C).

After drying at 60 °C, the films were annealed at 200 °C for 3 h under argon flow (100 mL/min) to improve contact and stabilize the baseline resistance. Gas-sensing measurements were carried out in a custom-built chamber equipped with a heater, thermocouple, and electrical feedthroughs (Figure S1, Supporting Information). The sensor resistance was monitored using a Keithley 2602 source meter. High-purity (99.999%) gases (Cryotech Vietnam) were diluted with dry air via mass flow controllers (MKS Instruments) to achieve the desired concentrations, maintaining the total flow rate at 400 sccm. Unless otherwise stated, all measurements were performed at room temperature (25 ± 1 °C).

Gas sensing measurements were performed using a static headspace injection method. Target TEA concentrations were generated by withdrawing saturated vapor from the headspace of a sealed source vial at 25 °C. The headspace concentration was determined by the saturated vapor pressure at 25 °C. For higher concentrations, a small, precise volume of this saturated vapor was injected into the test chamber using a calibrated microsyringe. To accurately achieve ppb-level concentrations, a two-stage volumetric serial dilution protocol was implemented. First, a known volume of the saturated headspace was withdrawn from the source vial and injected into an intermediate volume to achieve a primary dilution. Next, a microvolume of the resulting diluted concentration was withdrawn using a microsyringe and injected into the final sensing chamber. This cascade dilution approach allows for very low concentrations to be achieved with high precision and reproducibility.

The effect of relative humidity (RH) was studied using a humidity generator set to 40%, 60% and 80%. The effect of photoactivation was evaluated by comparing sensing measurements in darkness and under white light from an LED (C503D-WAN, Cree LED Inc., Durham, USA). The irradiance incident on the sensor was set to 67 mW/cm^2 using a calibrated luxmeter, so that it was equal to the average value of sunlight in Hanoi. The sensor response (S) was defined as R_a/R_g for reducing gases and R_g/R_a for oxidizing gases, where R_a and R_g represent the resistance in air and in the target gas, respectively. Response time (τ_{res}) was defined as the time to reach 90% of the maximum total resistance change upon gas exposure, and recovery time (τ_{rec}) as the time required to recover 90% of the resistance change.[5] Sensitivity was calculated according to the official guidelines recommended by the International Union of Pure and Applied Chemistry (IUPAC), as the slope of the response as a function of gas concentration.[21] The theoretical limit of detection (LoD) was determined according to the official guidelines recommended by the International Union of Pure and Applied Chemistry (IUPAC).[22] Mathematically, the LoD is defined as LoD = 3 σ/S, where σ represents the standard deviation of the baseline signal and S is the sensitivity at low concentrations near the origin. Although the lowest concentration tested experimentally was 5 ppb, this definition provides a mathematically rigorous and standardized estimate of the minimum concentration that can be detected. Similarly to LoD, the limit of quantification (LoQ) was calculated as 10 σ/S,[27] and represents the minimum concentration that can be not only detected but also quantified with a percent relative standard deviation (RSD) of 10%.

Downloaded from pubs.acs.org/aanmf6/article-pdf/9/33/16061/6652075/acsanm.6c02958.pdf by guest on 22 October 2026

https://doi.org/10.1021/acsanm.6c02958
ACS Appl. Nano Mater. 2026, 9, 16061−16074

3. RESULTS AND DISCUSSION

3.1. Morphology and Composition of Hybrid Nanomaterials

The morphology of the as-prepared ZnO and Cu-porphyrin/ZnO nanomaterials was investigated by SEM (Figure 2A,B).

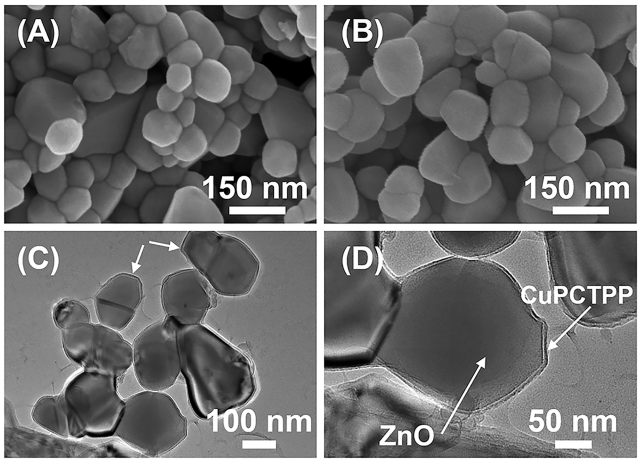


Figure 2. SEM images of (A) pristine ZnO nanoparticles and (B) Cu-porphyrin/ZnO nanohybrids. TEM images of Cu-porphyrin/ZnO nanohybrids at (C) lower and (D) higher magnification.

As shown in (Figure 2A), the ZnO sample consists of uniform nanoparticles with diameters in the range of 70−130 nm, which tend to assemble into loose aggregates. These morphological entities represent secondary nanostructures that are polycrystalline, composed of smaller interconnected primary crystalline domains, as will be detailed and quantified in the subsequent microstructural analysis. The formation process can be rationalized as follows: during hydrothermal treatment at low temperature, Zn^{2+} ions react with $(OH)^-$ species in the presence of CTAB micelles, which act as soft templates and favor nucleation. Subsequent heat treatment at 600 °C removes the surfactant and sharpens the particle morphology. As confirmed by Figure S2 (Supporting Information), annealing strongly reduces particle size compared to the rougher and larger preannealed ZnO spheres.

After surface modification with Cu-porphyrin, the overall ZnO morphology remains essentially unchanged (Figure 2B), since the organic layer is extremely thin and cannot be directly resolved by SEM.

TEM analysis (Figure 2C,D) shows the surface functionalization: a thin contrast layer surrounding the ZnO nanoparticles (indicated by the white arrows) can be distinguished, consistent with a conformal Cu-porphyrin coating.

Elemental mapping by EDS (Figure S3, Supporting Information) confirmed a homogeneous distribution of Zn, O, Cu and C, demonstrating successful functionalization of ZnO with the porphyrin derivative.

3.2. Microstructure Analysis

Figure S4 shows the XRD patterns of ZnO nanoparticles before (blue plot) and after annealing at 600 °C (red plot). The nonannealed ZnO shows two broad, poorly resolved humps, indicating its predominantly amorphous character. In contrast, the annealed sample displays several sharp diffraction peaks attributable to the hexagonal wurtzite structure, as per JCPDS reference 36−1451 (green bars),[23] with no detectable secondary phases or amorphous contributions. The average crystallite size, estimated from the Debye−Scherrer equation,[24] is 25.5 nm. This result confirms that particles with sizes between 70 and 130 nm observed by SEM are secondary aggregates, consisting of smaller and tightly coalesced primary single-crystalline domains. Crucially, this sub-30 nm size regime is directly comparable to twice the characteristic Debye length (λ_D) of ZnO at room temperature. In such nanoscale crystallite networks, electron transport is exquisitely sensitive to boundary potential fluctuations, ensuring that interfacial photoinduced charge transfer and target gas adsorption modulate the conduction channel throughout the entire volume of the primary nanoparticles.[25−27]

HRTEM images of the porphyrin-coated ZnO NPs confirm that the ZnO NPs remain unaffected, with an interplane distance of 0.25 nm corresponding to the (101) planes of the hexagonal ZnO, while SAED patterns confirm the crystalline nature of the nanoparticles (Figure S5).

3.3. Optical Properties

Figure 3A shows the UV−vis absorption spectra of ZnO and Cu-porphyrin/ZnO nanohybrids. The absorption edge of ZnO appears around 359 nm, typical of wurtzite ZnO,[28] with a slight blue shift compared to bulk ZnO, consistent with nanoscale size effects.[29]

Upon functionalization, additional absorption bands emerge in the visible range due to CuTPPCOOH. In particular, the band near 420 nm is broadened, indicating a partial aggregation of porphyrin onto the surface, in line with porphyrin film thickness observed with TEM.[30]

The Q-band at ∼546 nm is slightly suppressed due to the presence of the central Cu^{2+} ion, consistent with previous porphyrin reports.[31] These features confirm that the porphyrin molecules remain optically active and capable of absorbing visible light, which is expected to play a role in photoenhanced sensing.

Photoluminescence (PL) spectra of pristine ZnO and CuTPPCOOH/ZnO nanohybrids at room temperature are shown in (Figure 3B). Pure ZnO nanoparticles exhibit a dominant and sharp UV emission near the band edge (NBE) centered at 3.17 eV, which originates from the recombination of free excitons across the wide band gap of wurtzite ZnO. Additionally, a broad defect-related suppressed visible emission band centered around 2.15 eV is observed, accompanied by a small deep-level feature at 1.61 eV. The broad visible emission is conventionally attributed to radiative recombination involving intrinsic point defects, predominantly singly ionized oxygen vacancies (V_O^+), and surface states. Upon surface functionalization with CuTPPCOOH, a dramatic photoluminescence quenching is observed for both the NBE peak (3.17 eV) and defect-related visible emissions. This pronounced luminescence suppression demonstrates efficient photoinduced charge transfer across the CuTPPCOOH/ZnO heterojunction interface, experimentally validating a functional type-II energy band alignment in the synthesized hybrid. Rather than undergoing radiative excitonic recombination, photoexcited electrons are rapidly injected from the excited state of Cu-porphyrin into the ZnO conduction band, driven by a favorable interfacial energy gradient that leads to the spatial separation of photogenerated electron−hole pairs at the interface. Since interfacial charge separation occurs on a femtosecond to picosecond time scale, orders of magnitude faster than the nanosecond radiative recombination lifetime,

Downloaded from pubs.acs.org/aanmf6/article-pdf/9/33/16061/6652075/acsanm.6c02958.pdf by guest on 22 October 2026

https://doi.org/10.1021/acsanm.6c02958
ACS Appl. Nano Mater. 2026, 9, 16061−16074

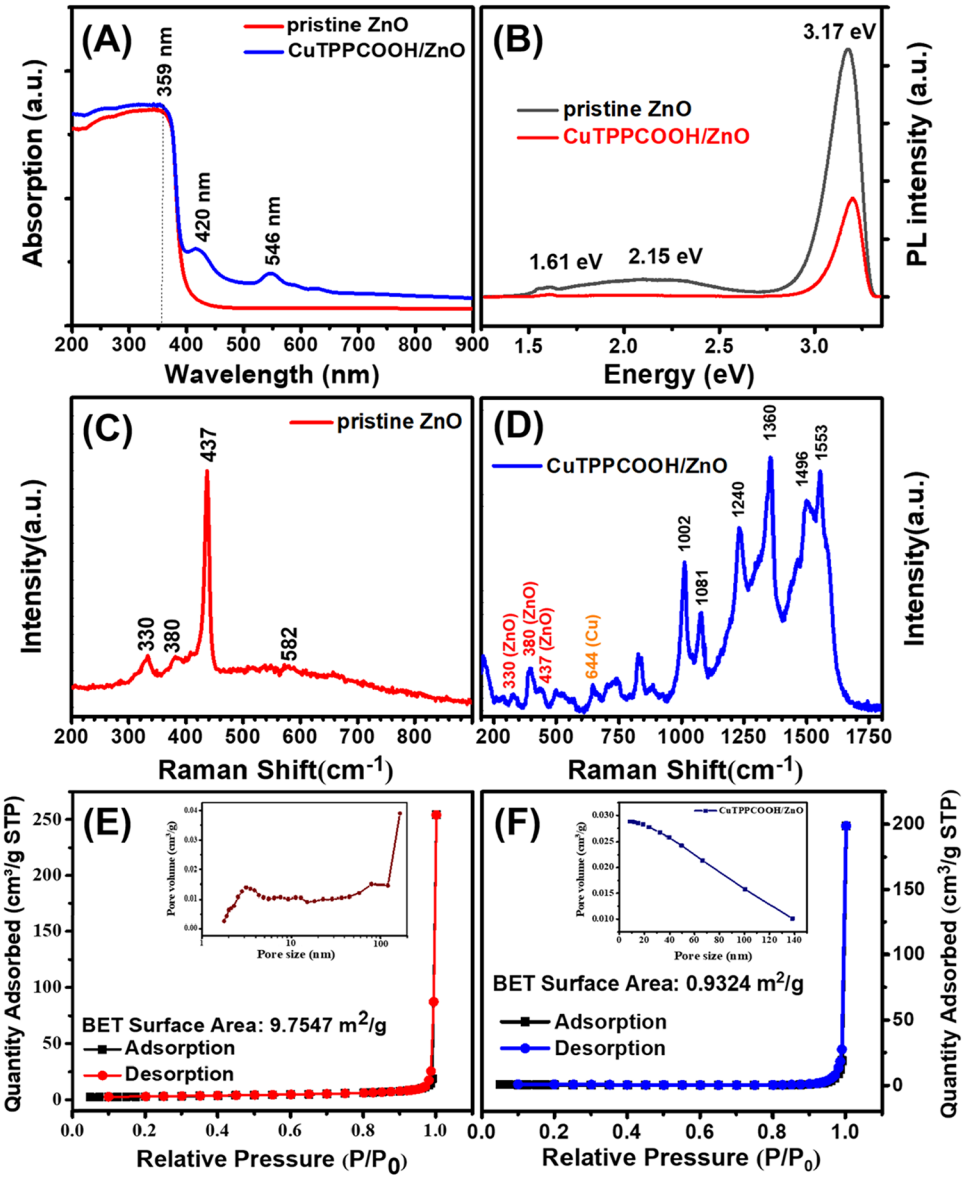


Figure 3. (A) UV−Vis spectra of pristine ZnO and Cu-porphyrin/ZnO nanohybrid; (B) PL spectra of pristine ZnO and Cu-porphyrin/ZnO nanohybrid; Raman spectra of (C) pristine ZnO and (D) Cu-porphyrin/ZnO nanohybrid; N_2 adsorption−desorption isotherms of (E) pristine ZnO and (F) Cu-porphyrin/ZnO nanohybrid.

radiative transitions are effectively suppressed. Additionally, the CuTPPCOOH itself exhibits negligible fluorescence due to its intrinsically ultrafast excited-state relaxation: upon Soret excitation, the Cu(II) porphyrin undergoes a porphyrin-to-metal charge transfer (CT) in 65 fs, followed by rapid conversion to the tripdoublet state (^{2}T) in 350 fs, effectively bypassing any radiative S_1 emission.[32]

Raman spectra (Figure 3C,D) provide complementary structural information. The Raman spectrum of pristine ZnO (Figure 3C) exhibits characteristic phonon modes of the wurtzite lattice,[33] including the prominent E_2^{high} mode at 437 cm^{-1}. After functionalization with CuTPPCOOH (Figure 3D), additional peaks appear that are attributed to the porphyrin framework.[34] Specifically, the bands at 1533, 1496, 1360, 1240, 1081, and 1002 cm^{-1} correspond to $\beta-\beta$ stretching (ν_2), phenyl ring vibration, $\alpha-\beta$ and $\alpha-$N stretching, Cm−Ph stretching (ν_1), pyrrole C$\beta-$H stretching, and combined pyrrole/phenyl modes, respectively.[35] The intensity of these porphyrin-related modes exceeds the strongest ZnO signal by almost three times. This signal amplification is attributed to the resonance Raman enhancement effect, triggered by the close alignment between the excitation laser wavelength and the electronic absorption Q-bands of the Cu-porphyrin complex.[36]

3.4. Porosity of the Nanomaterials

The textural properties were examined by N_2 adsorption−desorption isotherms (Figure 3E,F). Both ZnO and Cu-porphyrin/ZnO exhibit type III isotherms, consistent with weak adsorbent−adsorbate interactions. Pure ZnO nanoparticles display a BET surface area of 9.75 m^2/g, while the Cu-porphyrin/ZnO nanohybrid shows a reduced value of 0.93 m^2/g.

At first glance, this drastic decrease may appear counterintuitive since SEM/TEM reveal no significant change in particle morphology. However, the reduction in accessible surface area can be explained by partial coverage of interparticle pores by porphyrin molecules.[37] The organic

Downloaded from pubs.acs.org/aanmf6/article-pdf/9/33/16061/6652075/acsanm.6c02958.pdf by guest on 22 October 2026

https://doi.org/10.1021/acsanm.6c02958
ACS Appl. Nano Mater. 2026, 9, 16061−16074

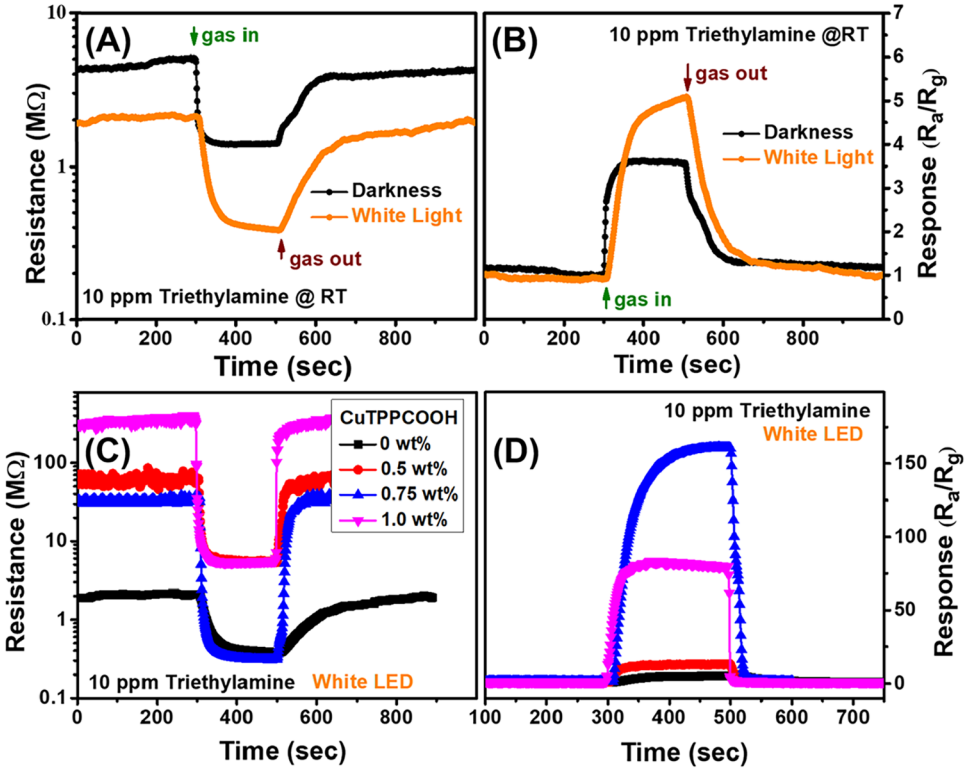


Figure 4. (A) Dynamic resistance and (B) sensor response of the ZnO sensor in darkness and under white LED illumination. (C) Dynamic resistance and (D) sensor response of the different nanohybrids to 10 ppm TEA at RT under white light.

coating tends to occupy interstitial voids between ZnO particles, limiting N_2 penetration during physisorption. This phenomenon has been reported for other organic−inorganic hybrids where thin functional layers reduce BET area without altering particle size.[38] Pore size distributions obtained via the BJH method support this interpretation: for bare ZnO, the pore volume distribution remains constantly low (~0.01 cm^3/g) from 3 to 100 nm and then increases sharply to ~0.04 cm^3/g above 100 nm. This trend confirms that the baseline porosity is predominantly governed by large interparticle macro-voids and crevices between the large annealed ZnO structures. In contrast, for the hybrid material, the volume of these large macropores is significantly suppressed, while a prominent contribution appears at narrower pore sizes, starting with a pore volume of 0.028 cm^3/g at 5 nm and decreasing linearly to 0.01 cm^3/g at 140 nm. This outcome quantitatively demonstrates that the bulky porphyrin macrocycles conformally occupy and plug the primary interstitial gaps, restricting physical N_2 access at cryogenic temperatures (77 K).[39] Importantly, this reduction in surface area does not negatively impact gas sensing properties. While N_2 physisorption purely probes the physical porosity at 77 K, chemiresistive sensing operates via chemical and electronic sensitization at room temperature under light activation. As detailed in the sensing mechanism section, the Cu-porphyrin layer provides a supramolecular recognition platform for TEA via π-stacking and dispersive interactions with the porphyrin macrocycle, while the square-planar Cu(II) center does not participate in axial coordination,[32] while simultaneously acting as a visible-light-harvesting antenna that injects photoexcited electrons into the ZnO lattice. Consequently, the superior supramolecular affinity and efficient photoinduced charge transfer at the hybrid heterojunction completely override the decrease in physical surface area, resulting in a significant improvement in sensing performance.[40]

3.5. Gas Sensing Performance

The $I-V$ curves of the hybrid sensor were measured at different temperatures (Figure S6), and the activation energy was extracted from the Arrhenius plot, consistent with thermally activated charge transport in ZnO-based systems.[41]

The detection performance of pristine ZnO was first evaluated in darkness and under white light by injecting 10 ppm of TEA (Figure 4A,B). The sensor showed the highest response under white light illumination, with a value of 5.1, compared to in darkness where the response was 3.6. The light emitted by the white LED corresponds to the absorption of porphyrins and therefore increased the response by 42%.

The RT sensing performance of the Cu-porphyrin/ZnO hybrids was then investigated as a function of CuTPPCOOH content (0, 0.5, 0.75, and 1.0 wt %) (Figure 4C,D). The general trend is for baseline resistance to increase with porphyrin loading, which is consistent with the organic layer introducing additional barriers to charge transport. Among the different compositions, the 0.75 wt % Cu-porphyrin sensor achieved the highest response (162 to 10 ppm TEA), suggesting an optimal balance between catalytic activity and charge transfer. At lower loadings, the number of active catalytic sites is limited, while at higher loadings excessive coverage may hinder electron injection and gas diffusion, leading to reduced performance.

The effect of TEA concentration was examined in the range 10−50 ppm (Figure 5). For all sensors, the response increased with increasing analyte concentration, as expected for surface-controlled adsorption processes. Again, the 0.75 wt % hybrid

https://doi.org/10.1021/acsanm.6c02958
ACS Appl. Nano Mater. 2026, 9, 16061−16074

Downloaded from pubs.acs.org/aanmf6/article-pdf/9/33/16061/6652075/acsanm.6c02958.pdf by guest on 22 October 2026

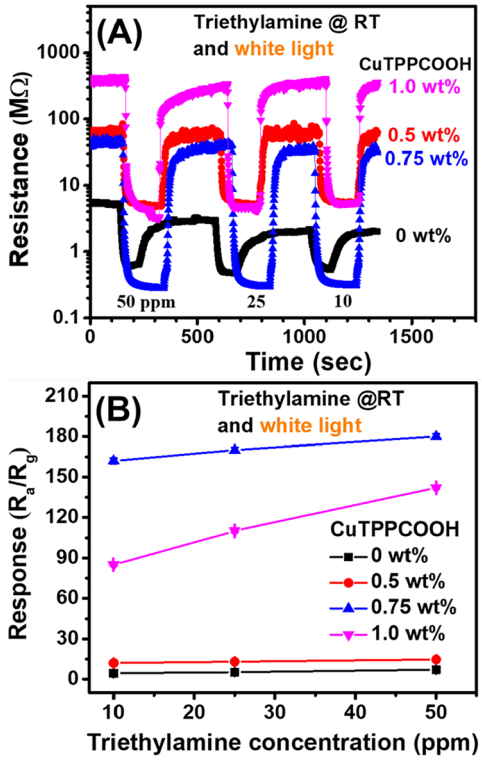


Figure 5. (A) Dynamic resistance and (B) response of hybrid sensors with different CuTPPCOOH contents.

outperformed the other loadings, confirming its optimized composition.

To clarify the synergistic role of illumination along with porphyrin functionalization, the optimized nanocomposite (0.75 wt % Cu-porphyrin/ZnO) was tested in darkness and under white light (Figure 6).

In ambient air and darkness, the pure ZnO sensor exhibits a baseline resistance of approximately 4.3 MΩ. After functionalization with 0.75 wt % CuTPPCOOH, the baseline resistance increases to approximately 640 MΩ. This increase results from electronic charge transfer at the organic/inorganic heterojunction, where porphyrins act as electron acceptors, depleting the ZnO conduction band and expanding the interfacial depletion layer and intergranular potential barriers. This high initial resistance plays a crucial role in amplifying gas sensing performance, as it provides a higher baseline from which reducing target gases can induce a greater decrease in relative resistance, and thus a greater response.

Under white light illumination, while the pure ZnO sensor shows only a marginal decrease from 4.3 MΩ to 2.1 MΩ, the baseline resistance of the hybrid nanocomposite decreases dramatically from about 640 MΩ in the dark to about 44 MΩ (about 14.5 times lower).

This improvement is attributed to photoexcitation of the surface-anchored porphyrins, which generate excitons that efficiently dissociate at the ZnO interface, injecting electrons into the conduction band, narrowing the depletion region, and significantly lowering the sensor's resistance.[42] This marked increase in photoconductivity serves as direct evidence of efficient interfacial charge separation, confirming that the electron injection pathway remains highly effective despite the molecular packing characteristics of the surface-bound macrocycles. Upon exposure to 50 ppm TEA, the response reached

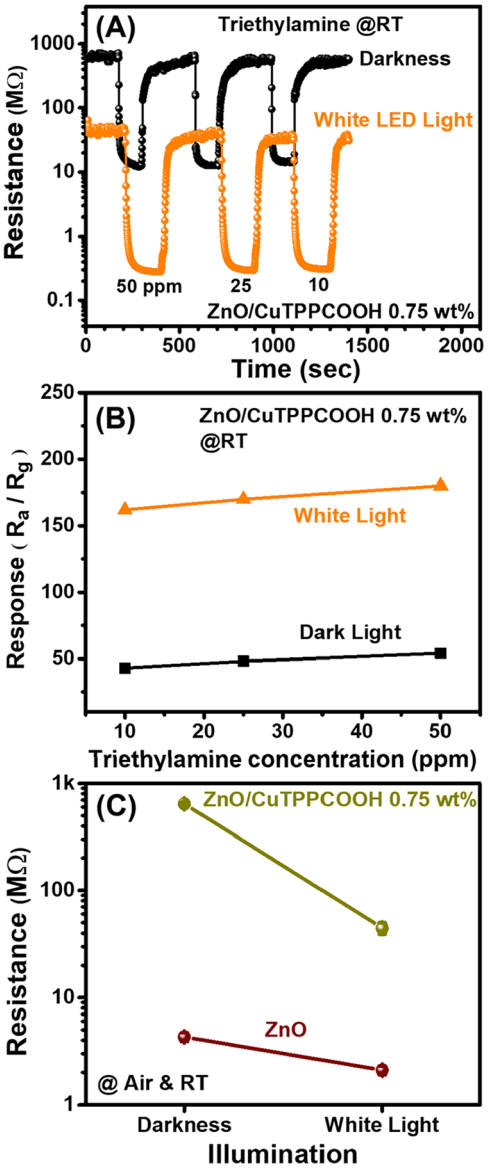


Figure 6. (A) Dynamic resistance and (B) response of the 0.75 wt % Cu-porphyrin/ZnO sensor under different illumination conditions; (C) baseline resistance of pristine ZnO and 0.75 wt % Cu-porphyrin/ZnO sensors under different illumination conditions.

~180 under illumination, more than three times the dark response (~50), underscoring the synergistic role of light activation and porphyrin sensitization.

The sensing characteristics were next investigated over a wider TEA concentration range (0.1−50 ppm) under both dark and white light illumination (Figure 7A). In both cases, the response increased monotonically with concentration and could be fitted by a Freundlich isotherm (Figure 7B), suggesting multilayer adsorption processes on the hybrid surface.

The sensitivity of the hybrid sensor, defined by the slope of the response/concentration curve (Figure 7B), is particularly high at low concentrations, allowing for the precise detection of trace amounts of TEA. As concentration increases, the slope gradually decreases, reflecting the progressive saturation of the available catalytic sites on the hybrid surface.

Under white light illumination, the sensor exhibits a steeper response curve than in darkness as seen by comparing the

Downloaded from pubs.acs.org/aanmf6/article-pdf/9/33/16061/6652097S/acsanm.6c02958.pdf by guest on 22 October 2026

https://doi.org/10.1021/acsanm.6c02958
ACS Appl. Nano Mater. 2026, 9, 16061−16074

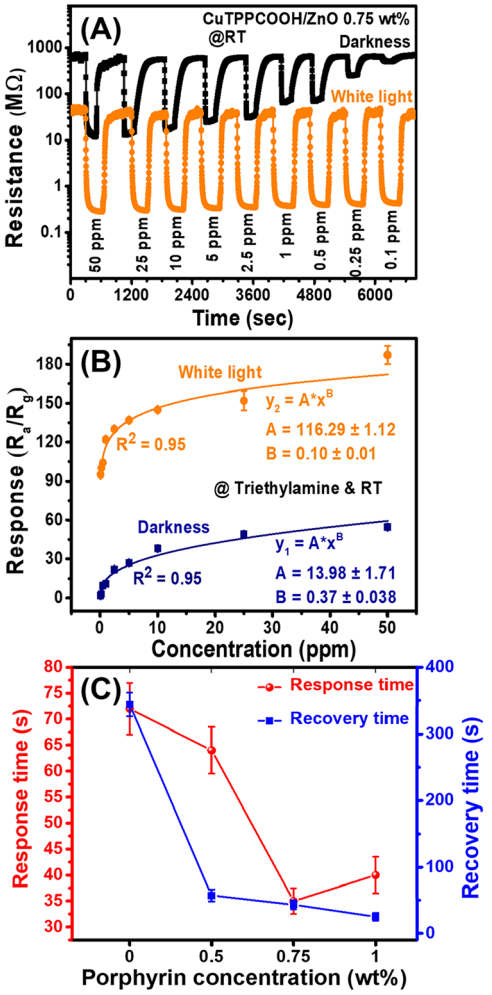


Figure 7. (A) Dynamic resistance and (B) response of the 0.75 wt % Cu-porphyrin/ZnO sensor as a function of TEA concentration with Freundlich fitting curve; (C) response and recovery times of hybrid sensors with different porphyrin content.

Freundlich isotherm exponents in (Figure 7B), indicating that photoactivation significantly increases sensitivity, especially at low concentrations, where it is most needed for safety monitoring.

Figure 7C shows that the 0.75 wt % sensor also exhibited the fastest response/recovery times dynamics (35/43 s at 10 ppm TEA under illumination), highlighting the beneficial role of optimal porphyrin coverage in facilitating rapid adsorption−desorption.

Since the response of the optimized sensor was found to be very high, its detection capability was further examined at subppm levels. As shown in (Figure 8A), measurable responses were obtained down to 5−80 ppb, with the calibration curve following the Freundlich law. The calculated limit of detection was ∼0.4 ppb, demonstrating the excellent detection capability of the hybrid system under white light illumination.

The influence of relative humidity was quantitatively evaluated in the 40−80% RH range (Figure S7). As detailed in Figure S7B, increasing humidity results in a negligible decrease in response, less than 5% (from 160.5 to 153.3), while maintaining fast recovery kinetics (21−24 s) and high baseline stability, confirming that sensor performance is not degraded at high humidity values.

The repeatability of the optimized hybrid was investigated by repeated exposures to 0.25 ppm TEA (Figure 9A), and long-term stability was assessed by repeating the test after 6 months (Figure 9B). During the 6-month period between the two tests, the sensors were stored in sealed, light-shielded containers equipped with a silica gel desiccant to prevent photobleaching and moisture-induced surface degradation. As shown in (Figure 9A), seven consecutive cycles produced consistent responses with minimal drift (average response of 92.8 ± 5.4). After six months (Figure 9B), the average response remained 87.7 ± 4.0, corresponding to 94.5 ± 9.8% retention of the initial value.

Reproducibility was also verified across five independent devices (Figure 9C), with an average response of 175.4 ± 5.7 and a relative variation of only 3.2%, demonstrating excellent device-to-device consistency.

Finally, the selectivity of the hybrid sensor was assessed against potential interfering gases (methanol, toluene, ethanol, isopropanol, acetone) at room temperature under white light (Figure 9D). The response to 50 ppm TEA (∼180) was substantially higher than that to other analytes, even when tested at higher concentrations (e.g., acetone 1000 ppm produced only $S \sim 85$).

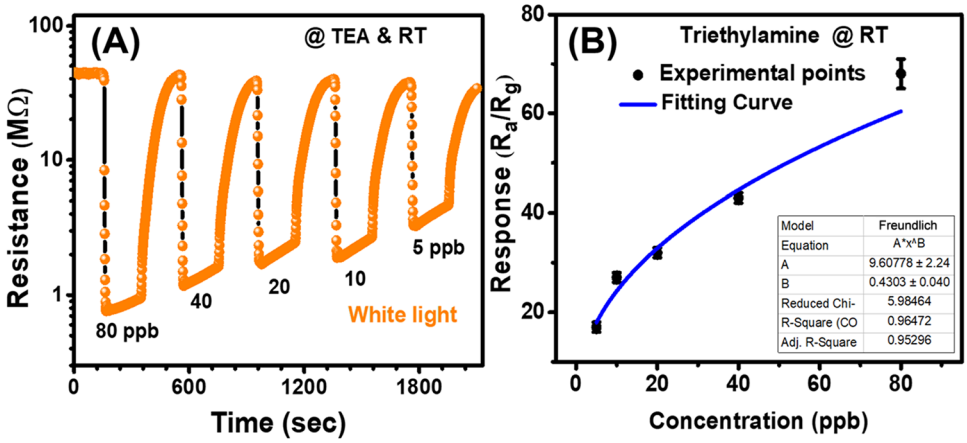


Figure 8. (A) Dynamic resistance and (B) response of the 0.75 wt % Cu-porphyrin/ZnO hybrid sensor at low TEA concentrations under white LED illumination.

Downloaded from pubs.acs.org/aanmf6/article-pdf/9/33/16061/6652975/acsanm.6c02958.pdf by guest on 22 October 2026

https://doi.org/10.1021/acsanm.6c02958
ACS Appl. Nano Mater. 2026, 9, 16061−16074

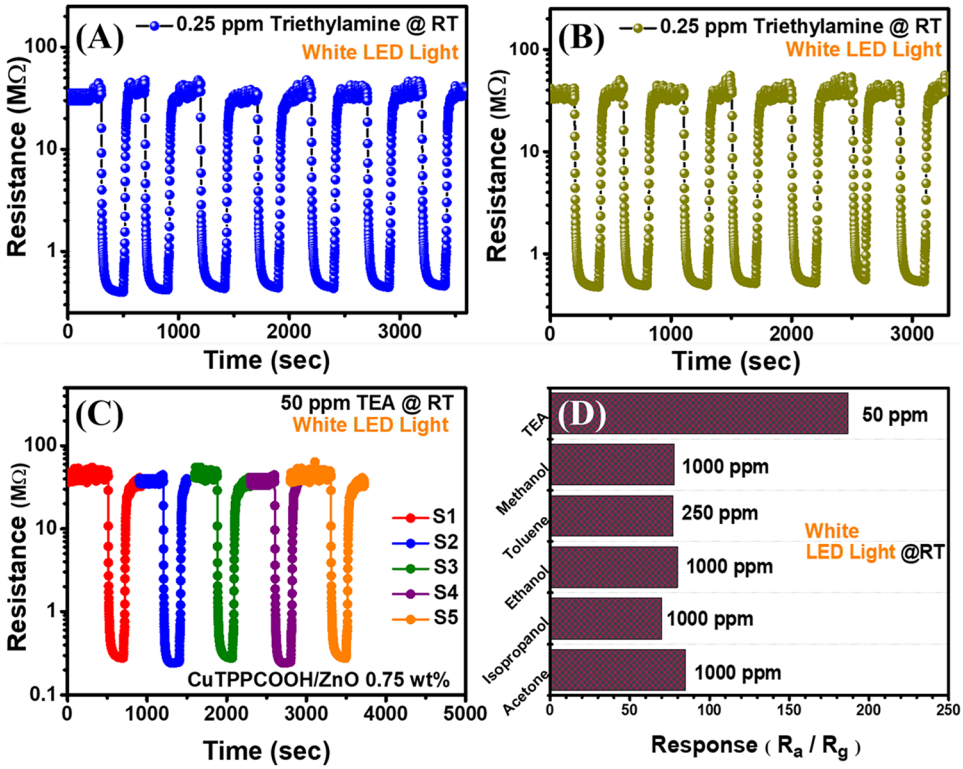


Figure 9. Performance of the 0.75 wt % Cu-porphyrin/ZnO hybrid sensor: (A) short-term repeatability; (B) long-term stability after six months; (C) dynamic resistance from five different sensors; (D) selectivity.

Table 1. Performance of Gas Sensors Based on Porphyrins

material	gas	conc. (ppm)	response	t_{res}/t_{rec} (s)	LoD (ppb)	refs
ZnTAP	NO_2	100	3.3	120/260	1000	43
p-HTClPP	NO_2	100	1.37	260/1080	5000	44
p-HTClPPCo			1.71	240/695	500	
SnO_2/ZnPP	toluene	9	15.9	260/220	20	45
ZnO/CoPP			3.5			
porphyrin-based HOF	NO_2	0.1	1.07	17.6/15.4	40	46
NGO/CoTPyrP	NO_2	0.05	22.15	50/229 (5 ppm)	6	47
	SO_2	0.25	3.35	43/262 (15 ppm)	74	
	NH_3	2	7.31	41/129 (25 ppm)	113	
	H_2S	0.25	3.02	45/205 (15 ppm)	178	
La (TBPP)(TBNc)	acetone	100	1.57	53/78	200	48
TiOTPyP nanofiber/SWCNT	H_2O_2	10	1.51	16/2	2	49
RGO/Eu (TPyP)(Pc)	NO_2	100	1.16	172/828 (20 ppm)	80	50
Eu (TPyP) {Pc-$(OC_8H_{17})_8$}	NO_2	100	13.81	110/240	1000	51
CoT[$(Pyr)_4$] P	NO_2	0.4	1.08 (45% RH)	>120/>540	50	52
Cu(F_{16}Pc)/pNiDPP	NH_3	20	1.08	162/552 (90 ppm)	228	53

Table 2. Triethylamine Gas Sensing Performance of MOS Material-Based Sensors

material	conc. (ppm)	response (R_{air}/R_{gas})	t_{res}/t_{rec} (s)	temp (°C)	LoD (ppb)	refs
Ag-decorated Zn_2SnO_4	50	83.6	1/20	220	1000	57
ZnO/$ZnFe_2O_4$	100	40.15	32/41	200	-	58
MoS_2/ZnO	100	23.57	103/134	200	-	59
Co-doped ZnO	50	68.0	8/16	280	200	60
ZnO/ZFO	100	78	11/103	240	500	61
Ru-SnMOF@SnO_2	100	688.6	4/87	250	-	62
ZnS@ZnO	100	74.65	3/176	200	1000	63

While the sensor demonstrates excellent discrimination against the tested interfering VOCs (methanol, ethanol, isopropanol, toluene, and acetone), further cross-reactivity studies with lighter alkaline interfering gases such as ammonia (NH_3) represent an important direction for future research. From a fundamental point of view, the superior response to

https://doi.org/10.1021/acsanm.6c02958
ACS Appl. Nano Mater. 2026, 9, 16061−16074

Downloaded from pubs.acs.org/aanmf6/article-pdf/9/33/16061/6652075/acsanm.6c02958.pdf by guest on 22 October 2026

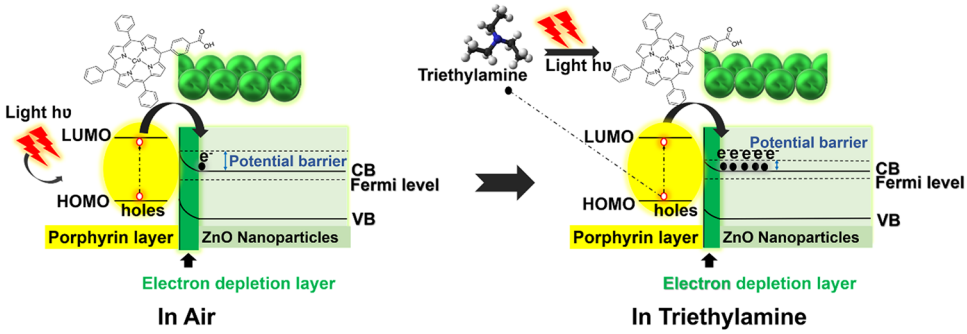


Figure 10. Schematic illustration of the TEA sensing mechanism in Cu-porphyrin/ZnO hybrids under illumination.

TEA compared to simpler basic molecules such as NH_3 is driven by its significantly lower ionization potential (~7.5 eV versus ~10.1 eV for NH_3) and the strong electron-donating effect of its three alkyl chains, which promotes efficient electron injection into the conduction band of ZnO during surface interaction.

3.6. Comparison with Literature

Tables 1 and 2 summarize recent results on porphyrin-based sensors and metal oxide semiconductor sensors for TEA, respectively.

Table 1 highlights the performance of porphyrin-based sensors toward different gases. Most of these systems operate at room temperature but exhibit relatively modest responses (typically <20) and limits of detection in the ppb−ppm range. Comparatively, our Cu-porphyrin/ZnO hybrid achieves a response of 162 to 10 ppm TEA with a theoretical limit of detection of 0.4 ppb, which is substantially higher than other porphyrin systems reported to date.

Table 2 compares MOX-based sensors for TEA detection. While some advanced heterostructures, such as Ru-SnMOF@SnO_2, exhibit very high responses at elevated temperatures, most MOX systems require operating temperatures of 200−300 °C and show low responses. In contrast, the Cu-porphyrin/ZnO sensor presented here achieves high performance at room temperature without external heating, making it highly advantageous for low-power, portable applications.

Conventional MOX sensors operating at these high temperatures continuously consume between 100 and 500 mW due to high thermal dissipation on ceramic substrates.[54] Even state-of-the-art microhot plates require a continuous power budget of 10−50 mW to maintain thermal activation of the sensing layer.[55,56] In contrast, our hybrid light-activated architecture completely avoids thermal activation and, using a miniature micro-LED placed directly above the sensor, would require less than 5.6 mW. Furthermore, because optical excitation undergoes instantaneous modulation without the thermal inertia typical of hot plates, a duty-cycling protocol can be easily implemented. By turning on the micro-LED for 100 ms every 1 s, average power consumption is reduced to <0.56 mW. Furthermore, because the operating irradiance used was intentionally matched to natural sunlight, this system could operate with only sunlight during daylight hours, further reducing power consumption.

A notable feature of our system is that the optimal porphyrin loading (0.75 wt %) provides both high response and short response/recovery times, positioning the Cu-porphyrin/ZnO hybrid among the most efficient MOS-based TEA sensors reported to date, especially under light activation.

3.7. Proposed Sensing Mechanism

The detection mechanism of the Cu-porphyrin/ZnO hybrid sensor is schematically illustrated in (Figure 10).

The interface between ZnO and Cu-porphyrin forms a heterojunction due to their different work functions. Thermodynamic analysis confirms the formation of a type-II heterojunction: the LUMO level of the Cu-porphyrin is located at approximately −3.7 eV (vs vacuum),[64] while the conduction band of ZnO lies at approximately −4.2 eV.[65] This energetic offset creates a spontaneous driving force that facilitates the transfer of photoexcited electrons from the porphyrin into the ZnO lattice.

This leads to band bending at the interface, facilitating charge separation. Under illumination, Cu-porphyrin molecules absorb visible light, generating excitons. At the interface, these excitons dissociate, with electrons transferred into the conduction band of ZnO and holes remaining in the porphyrin layer. Notably, although the UV−vis analysis indicated H-type molecular aggregation on the oxide surface (evidenced by the broadening and blue-shift of the Soret band),[50] the typical exciton self-quenching associated with such face-to-face packing is effectively bypassed by favorable interfacial kinetics: electron injection from photoexcited porphyrin into the ZnO conduction band occurs in femtosecond to picosecond, orders of magnitude faster than the nonradiative deactivation pathways within the H-aggregates, which require nanoseconds. As a result, interfacial charge separation outcompetes the self-quenching process, which is macroscopically manifested by the pronounced drop in baseline resistance observed when switching from darkness to white light (Figure 6).

This process increases the baseline conductance of the sensor and provides additional active carriers for gas interactions.[28] The alignment lowers the energy barrier between ZnO and Cu-porphyrin, shortening the response and recovery times.[67] In ambient air, oxygen molecules adsorb onto ZnO and capture electrons, forming O_2^- species at room temperature. This process creates surface depletion layers and increases resistance.

When the sensor is exposed to TEA, the gas molecules adsorb onto the Cu-porphyrin surface via supramolecular interactions (primarily dispersive forces due to ethyl groups and π-stacking with the porphyrin macrocycle), rather than through axial coordination to the Cu(II) center, which retains its square-planar geometry.[32] This interpretation is strongly supported by recent DFT calculations showing that triethylamine exhibits the highest adsorption affinity on free-base porphyrins via noncovalent interactions with the conjugated macrocycle, without requiring a metal center for recognition.[66] The strong electron-donating character of TEA, arising from

Downloaded from pubs.acs.org/aanmf6/article-pdf/9/33/16061/6652075/acsanm.6c02958.pdf by guest on 22 October 2026

https://doi.org/10.1021/acsanm.6c02958
ACS Appl. Nano Mater. 2026, 9, 16061−16074

the inductive effect of its three ethyl groups, promotes efficient electron transfer from the adsorbed TEA molecule to the porphyrin π-system and subsequently to the ZnO conduction band. These injected electrons neutralize the adsorbed oxygen species (O_2^-) on the ZnO surface, reducing the depletion layer width and thereby decreasing the sensor resistance. This mechanism is consistent with the observed decrease in resistance upon TEA exposure and is further supported by the low ionization potential of TEA (~7.5 eV), which facilitates charge donation.

Crucially, the photoinduced charge separation at the heterojunction generates an oxidized porphyrin state ($P^{\bullet+}$) upon electron injection into ZnO. This oxidized porphyrin acts as a strong electron acceptor that can be readily reduced by the electron-rich TEA molecule, thereby regenerating the neutral porphyrin and closing a photocatalytic cycle. This regenerative mechanism ensures sustained photocurrent generation under continuous illumination and amplifies the overall sensor response, as the porphyrin acts as a catalytic mediator for electron transfer from TEA to the ZnO conduction band. Importantly, this cycle is fully consistent with the reversible nature of the sensor response: upon removal of TEA from the atmosphere, the adsorption equilibrium shifts toward desorption, and the porphyrin returns to its neutral state, restoring the initial baseline resistance. The reversibility is further supported by the noncovalent nature of the TEA-porphyrin interaction, which does not involve irreversible chemical bond formation.

To quantitatively reconcile the 10-fold decrease in geometric surface area with the sharp increase in TEA sensitivity, we must consider the transition from a linear physical parameter (surface area) to an exponential electronic process. In polycrystalline chemiresistors, charge transport is governed exponentially by the Schottky barrier height ($e\Delta\Phi$) at the grain boundaries[67]

$$R = R_0 \exp\left(\frac{e\Delta\Phi}{k_B T}\right)$$

Due to the small size of ZnO crystallites (approximately 25.5 nm), even small changes in surface charge translate into enormous changes in conductivity. At 298 K (k_BT approximately 25.7 meV), the boundary barrier modulation ($\Delta(e\Delta\Phi)$) required to achieve our experimental response ($S = R_a/R_g = 162$) can be calculated as

$$\Delta(e\Delta\Phi) = k_B T \ln(S) = 25.7\ \text{meV} \times \ln(162) \approx 130.8\ \text{meV}$$

A change of only approximately 131 meV is easily induced by the strong electron-donating character of TEA, which arises from the inductive effect of its three ethyl groups and its low ionization potential (~7.5 eV). Since the sensor response scales exponentially with this energy barrier, this electronic sensitization completely dominates the linear 10-fold reduction in physical surface area measured at 77 K. The incorporation of Cu-porphyrin improves the sensing response toward TEA compared to pristine ZnO nanoparticles, especially under white LED light illumination.[68] The improved performance arises from the synergistic combination of the visible-light-harvesting ability of the porphyrin, which generates additional photogenerated charge carriers, the type-II heterojunction that facilitates efficient charge separation and electron injection into ZnO, the selective supramolecular recognition of TEA by the porphyrin macrocycle, and the photocatalytic cycle in which the oxidized porphyrin ($P^{\bullet+}$) is regenerated by electron donation from TEA, ensuring sustained sensor response under continuous illumination. The synergy between heterojunction band engineering, photoactivation, and supramolecular recognition explains the markedly improved sensing behavior, faster dynamics, and ultralow limit of detection compared to pristine ZnO.

4. CONCLUSIONS

In summary, we have successfully developed a high-performance, visible-light-activated gas sensor by engineering a nanoscale hybrid heterojunction between wurtzite ZnO nanoparticles and surface-anchored Cu-porphyrin derivatives. This work addresses the critical bottleneck of metal oxide chemiresistors (namely, the high-power consumption required for thermal activation) by demonstrating that efficient room-temperature operation is achievable through rational surface nanofunctionalization.

The synergistic coupling of the photoactive CuTPPCOOH layer with the nanocrystalline ZnO network enables a highly efficient photoinduced charge transfer mechanism. Because the electrical transport is governed by Schottky barriers between adjacent ~25 nm grains, even subtle photoinduced shifts in carrier concentration produce orders-of-magnitude resistance modulations. This process drastically amplifies the sensor response under visible light illumination, yielding an ultralow theoretical limit of detection of 0.4 ppb and a remarkable response of 162 toward 10 ppm TEA, values that significantly outperform pristine ZnO and existing state-of-the-art sensors. Furthermore, the hybrid device exhibits excellent selectivity, rapid response/recovery dynamics (~40 s), and robust stability against moisture. Although the sensor exhibits high TEA selectivity over interfering VOCs and strong humidity tolerance (40%−80% RH), real-world applications involve complex, multicomponent gas mixtures. For practical use in unpredictable, multigas environments, integrating this hybrid sensor into multisensor arrays or using dynamic light pulse protocols will provide the necessary pattern recognition capability to deconvolve complex matrices.

From a broader perspective, this study provides a validated pathway for the design of low-power, light-driven sensing platforms. The combination of simple wet-chemical synthesis, scalable fabrication, and room-temperature operability makes this hybrid architecture an ideal candidate for integration into next-generation portable monitoring systems and wearable safety devices for the real-time detection of hazardous volatile organic compounds.

■ ASSOCIATED CONTENT

Supporting Information

The Supporting Information is available free of charge at https://pubs.acs.org/doi/10.1021/acsanm.6c02958.

Schematic of the gas sensing measurement setup; SEM images of pristine and functionalized ZnO, SEM, EDS spectra and elemental mapping of hybrid material; XRD patterns of pristine ZnO; TEM and SAED images, temperature-dependent $I-V$ characterization curves and Arrhenius plot of the hybrid material, nanohybrid sensor performance under different humidity conditions (DOCX)

Downloaded from pubs.acs.org/aanmf6/article-pdf/9/33/16061/6652075/acsanm.6c02958.pdf by guest on 22 October 2026

https://doi.org/10.1021/acsanm.6c02958
ACS Appl. Nano Mater. 2026, 9, 16061−16074

AUTHOR INFORMATION

Corresponding Authors

Matteo Tonezzer − *IMEM-CNR, Sede di Trento—FBK, Povo, TN 38123, Italy;* orcid.org/0000-0003-4694-4181; Email: matteo.tonezzer@cnr.it

Corrado Di Natale − *Department of Electronic Engineering, University of Rome Tor Vergata, 00133 Rome, Italy; Centre for Interdisciplinary Research (CIDR), SRM University-AP, Amaravati, Andhra Pradesh 522502, India;* orcid.org/0000-0002-0543-4348; Email: dinatale@uniroma2.it

Authors

Van Duy Lai − *Department of Electronic Engineering, University of Rome Tor Vergata, 00133 Rome, Italy; Research and Innovation Centre, Fondazione Edmund Mach, San Michele all' Adige, TN 38098, Italy; Institute of Materials Science, Vietnam Academy of Science and Technology, 10072 Hanoi, Vietnam*

Thi Nguyet To − *Univ. Lille, CNRS, Univ. Polytechnique Hauts-de-France, UMR 8520—IEMN, F-59000 Lille, France*

Valerio Allegra − *Department of Electronic Engineering, University of Rome Tor Vergata, 00133 Rome, Italy*

Roberto Paolesse − *Department of Chemical Science and Technology, University of Rome Tor Vergata, 00133 Rome, Italy;* orcid.org/0000-0002-2380-1404

Gabriele Magna − *Department of Chemical Science and Technology, University of Rome Tor Vergata, 00133 Rome, Italy;* orcid.org/0000-0003-2140-0110

Franco Biasioli − *Research and Innovation Centre, Fondazione Edmund Mach, San Michele all' Adige, TN 38098, Italy*

Alexandro Catini − *Department of Electronic Engineering, University of Rome Tor Vergata, 00133 Rome, Italy*

Complete contact information is available at: https://pubs.acs.org/10.1021/acsanm.6c02958

Notes

The authors declare no competing financial interest.

ACKNOWLEDGMENTS

V.D.L. acknowledges the support of Fondazione Edmund Mach and the University of Rome Tor Vergata for his PhD scholarship.

REFERENCES

(1) Cheng, S.; Chang-Chien, G. P.; Huang, Q.; Zhang, Y.-B.; Yan, P.; Zhang, J.; et al. Global Research Trends in Health Effects of Volatile Organic Compounds during the Last 16 Years: A Bibliometric Analysis. *Aerosol Air Qual. Res.* **2019**, *19* (8), 1834−1843.

(2) National Toxicology Program. Technical Report on the Toxicity Studies of Triethylamine (CASRN 121−44−8) 2018 https://www.ncbi.nlm.nih.gov/books/NBK551108/ accessed on June 14th, 2026.

(3) American Conference of Governmental Industrial Hygienists (ACGIH). Triethylamine 2026 https://www.acgih.org/triethylamine accessed on June 14th, 2026

(4) National Center for Biotechnology Information. PubChem Compound Summary for CID 8471, Triethylamine 2026 https://pubchem.ncbi.nlm.nih.gov/compound/Triethylamine accessed on June 14th 2026.

(5) John, R. A. B.; Kumar, A. R. A Review on Resistive-Based Gas Sensors for the Detection of Volatile Organic Compounds Using Metal-Oxide Nanostructures. *Inorg. Chem. Commun.* **2021**, *133*, No. 108893.

(6) Singh, A.; Sikarwar, S.; Verma, A.; Yadav, B. C. The Recent Development of Metal Oxide Heterostructures Based Gas Sensor, Their Future Opportunities and Challenges: A Review. *Sens. Actuators, A* **2021**, *332*, No. 113127.

(7) Tonezzer, M.; Le, D. T. T.; Duy, L. V.; Hoa, N. D.; Gasperi, F.; Van Duy, N.; Hieu, N. V. Electronic Noses Based on Metal Oxide Nanowires: A Review. *Nanotechnol. Rev.* **2022**, *11* (1), 897−931.

(8) Seekaew, Y.; Kamlue, S.; Wongchoosuk, C. Room-Temperature Ammonia Gas Sensor Based on Ti_3C_2Tx MXene/Graphene Oxide/CuO/ZnO Nanocomposite. *ACS Appl. Nano Mater.* **2023**, *6* (10), 9008−9020.

(9) Gu, G.; Zhou, W.; Gao, Y.; Lv, Y.; Yang, X.; Liao, C.; Yu, N.; Xu, J.; Gao, Y.; Lu, G. Spatially Binary Single-Atom La and Mn Sites on Co_3O_4 for Enhanced Triethylamine Sensing. *ACS Sens.* **2026**, *11* (6), 2207−2217.

(10) Zhang, Y.; Wang, M.-Y.; San, X.-G.; Shen, Y.-B.; Wang, G.-S.; Zhang, L.; Meng, D. $Ti_3C_2T_x/SnO_2$ P−N heterostructure construction boosts room temperature detecting formaldehyde. *Rare Met.* **2024**, *43* (1), 267−279.

(11) Hu, J.-Y.; Lei, H.; Zhang, H.-Y.; Xue, X.-X.; Wang, X.-P.; Wang, C.-H.; Zhang, Y. High reliable gas sensor based on crystal-facet regulated α-Fe_2O_3 nanocrystals for rapid detection of exhaled acetone. *Rare Met.* **2024**, *43* (12), 6500−6515.

(12) Ding, Y.; Du, B.; Guo, X.; Dong, Y.; Zhang, M.; Jin, W.; Gao, C.; Peng, D.; He, Y. An ultrasensitive NO_2 gas sensor based on a NiO-SnO_2 composite with a sub-ppb detection limit at room temperature. *Sens. Actuators, B* **2024**, *414*, No. 135916.

(13) Wang, Y.-X.; Liu, B.; Liu, B.-H.; Zhang, Y. Oxygen-assisted recoverable hydrogen sensor based on sensing gate field effect transistor with ppb-level detection ability. *Rare Met.* **2025**, *44* (2), 1160−1169.

(14) Zhu, L.-Y.; Ou, L.-X.; Mao, L.-W.; Wu, X.-Y.; Liu, Y.-P.; Lu, H.-L. Advances in Noble Metal-Decorated Metal Oxide Nanomaterials for Chemiresistive Gas Sensors: Overview. *Nano-Micro Lett.* **2023**, *15* (1), No. 89.

(15) Kang, Y.; Kim, K.; Cho, B.; Kwak, Y.; Kim, J. Highly Sensitive Detection of Benzene, Toluene, and Xylene Based on CoPP-Functionalized TiO_2 Nanoparticles with Low Power Consumption. *ACS Sens.* **2020**, *5* (3), 754−763.

(16) Cordones, A. A.; Das Pemmaraju, C.; Lee, J. H.; Zegkinoglou, I.; Ragoussi, M.-E.; Himpsel, F. J.; de la Torre, G.; Schoenlein, R. W. Excited-State Charge Distribution of a Donor−π−Acceptor Zn Porphyrin Probed by N K-Edge Transient Absorption Spectroscopy. *J. Phys. Chem. Lett.* **2021**, *12* (4), 1182−1188.

(17) Paolesse, R.; Nardis, S.; Monti, D.; Stefanelli, M.; Di Natale, C. Porphyrinoids for Chemical Sensor Applications. *Chem. Rev.* **2017**, *117* (4), 2517−2583.

(18) La, D. D.; Lai, D. V.; Quan, N. T. M.; Nguyen, H. H.; Van Le, H.; Van Tran, C.; Magna, G.; et al. Enhanced Photocatalytic Performance of ZnO Nanoparticles Functionalized with 5-(4′-carboxyphenyl)-10,15,20-triphenylporphyrin-zinc. *Mater. Res. Bull.* **2025**, *185*, No. 113326.

(19) Hu, C.; Jiang, D.; Zhang, Y.; Gao, H.; Zeng, Y.; Khaorapapong, N.; Liu, Z.; Yamauchi, Y.; Pan, M. Porphyrins-Based Multidimensional Nanomaterials: Structural Design, Modification and Applications. *Coord. Chem. Rev.* **2025**, *523*, No. 216264.

(20) Magna, G.; Muduganti, M.; Stefanelli, M.; Sivalingam, Y.; Zurlo, F.; Di Bartolomeo, F.; Catini, A.; Martinelli, E.; Paolesse, R.; Di Natale, C. Light-Activated Porphyrinoid-Capped Nanoparticles for Gas Sensing. *ACS Appl. Nano Mater.* **2021**, *4* (1), 414−424.

(21) IUPAC Compendium of Chemical Terminology. *Sensitivity*, 5th ed.; International Union of Pure and Applied Chemistry, 2025 DOI: 10.1351/goldbook.S05606.

(22) IUPAC Compendium of Chemical Terminology. *Limit of Detection*, 5th ed.; International Union of Pure and Applied Chemistry, 2025 DOI: 10.1351/goldbook.L03540.

Downloaded from pubs.acs.org/aanmf6/article-pdf/9/33/16061/6652075/acsanm.6c02958.pdf by guest on 22 October 2026

(23) Shatnawi, M.; Alsmadi, A. M.; Bsoul, I.; Salameh, B.; Mathai, M.; Alnawashi, G.; Alzoubi, G. M.; Al-Dweri, F.; Bawa'aneh, M. S. Influence of Mn Doping on the Magnetic and Optical Properties of ZnO Nanocrystalline Particles. *Results Phys.* **2016**, *6*, 1064−1071.
(24) Mustapha, S.; Ndamitso, M. M.; Abdulkareem, A. S.; Tijani, J. O.; Shuaib, D. T.; Mohammed, A. K.; Sumaila, A. Comparative Study of Crystallite Size Using Williamson-Hall and Debye-Scherrer Plots for ZnO Nanoparticles. *Adv. Nat. Sci.: Nanosci. Nanotechnol.* **2019**, *10* (4), No. 045013.
(25) Yamazoe, N.; Shimanoe, K. Fundamentals of Semiconductor Gas Sensors. In *Semiconductor Gas Sensors*, 2nd ed.; Woodhead Publishing, 2020; pp 3 38 DOI: 10.1016/B978-0-08-102559-8.00001-X.
(26) Kolmakov, A.; Moskovits, M. Chemical Sensing and Catalysis by One-Dimensional Metal-Oxide Nanostructures. *Annu. Rev. Mater. Res.* **2004**, *34*, 151−180.
(27) Torkamani Cheriani, M.; Mirzaei, A.; Kim, J.-H. Resistive-Based Nanostructured CeO_2 Gas Sensors: A Review. *Chemosensors* **2025**, *13* (8), No. 298.
(28) Samuel, M. S.; Bose, L.; George, K. C. Optical Properties of ZnO Nanoparticles. *Acad. Rev.* **2009**, *16* (1−2), 57−65.
(29) Fakhari, S.; Jamzad, M.; Kabiri Fard, H. Green Synthesis of Zinc Oxide Nanoparticles: A Comparison. *Green Chem. Lett. Rev.* **2019**, *12* (1), 19−24.
(30) Hestand, N. J.; Spano, F. C. Expanded theory of H- and J-Molecular Aggregates: The Effects of Vibronic Coupling and Intermolecular Charge Transfer. *Chem. Rev.* **2018**, *118* (15), 7069−7163.
(31) Liao, M.-S.; Scheiner, S. Electronic structure and bonding in metal porphyrins, metal = Fe, Co, Ni, Cu, Zn. *J. Chem. Phys.* **2002**, *117*, 205−219.
(32) Ha-Thi, M.-H.; Shafizadeh, N.; Poisson, L.; Soep, B. An Efficient Indirect Mechanism for the Ultrafast Intersystem Crossing in Copper Porphyrins. *J. Phys. Chem. A* **2013**, *117* (34), 8111−8118.
(33) Cuscó, R.; Alarcón-Llado, E.; Ibanez, J.; Artus, L.; Jimenez, J.; Wang, B.; Callahan, M. J. Temperature dependence of Raman scattering in ZnO. *Phys. Rev. B* **2007**, *75*, No. 165202.
(34) Lian, W.; Sun, Y.; Wang, B.; Shan, N.; Shi, T. Synthesis and properties of 5,10,15,20-tetra(4-(3,5-dioctoxybenzamidephenyl) porphyrin and its metal complexes. *J. Serb. Chem. Soc.* **2012**, *77*, 335−348.
(35) Gorski, A.; Starukhin, A.; Stavrov, S.; Gawinkowski, S.; Waluk, J. Resonance Raman spectroscopy study of protonated porphyrin. *Spectrochim. Acta, Part A* **2017**, *173*, 350−355.
(36) Moutinho, M. V. O.; Eliel, G. S. N.; Righi, A.; Gontijo, R. N.; Paillet, M.; Michel, T.; Chiu, P.-W.; Venezuela, P.; Pimenta, M. A. Resonance Raman Enhancement by the Intralayer and Interlayer Electron-Phonon Processes in Twisted Bilayer Graphene. *Sci. Rep.* **2021**, *11* (1), No. 17206.
(37) Zhang, T.; Ge, Y.; Wang, X.; Chen, J.; Huang, X.; Liao, Y. Polymeric Ruthenium Porphyrin-Functionalized Carbon Nanotubes and Graphene for Levulinic Ester Transformations into γ-Valerolactone and Pyrrolidone Derivatives. *ACS Omega* **2017**, *2*, 3228−3240.
(38) Liu, J.; Yang, Q.; Zhang, L.; Yang, H.; Gao, J.; Li, C. Organic−Inorganic Hybrid Hollow Nanospheres with Microwindows on the Shell. *Chem. Mater.* **2008**, *20* (13), 4268−4273.
(39) Kujawa, J.; Al-Gharabli, S.; Wrzeszcz, G.; Knozowska, K.; Lagzdins, R.; Talik, E.; Dziedzic, A.; Loulergue, P.; Szymczyk, A.; Kujawski, W. Physicochemical and magnetic properties of functionalized lanthanide oxides with enhanced hydrophobicity. *Appl. Surf. Sci.* **2021**, *542*, No. 148563.
(40) Sharma, A.; Eadi, S. B.; Noothalapati, H.; Otyepka, M.; Lee, H.-D.; Jayaramulu, K. Porous materials as effective chemiresistive gas sensors. *Chem. Soc. Rev.* **2024**, *53*, 2530−2577.
(41) IUPAC Compendium of Chemical Terminology. *Arrhenius Equation*, 5th ed.; International Union of Pure and Applied Chemistry, 2025 DOI: 10.1351/goldbook.A00446.
(42) Lan, M.; Zhao, H.; Yuan, H.; Jiang, C.; Zuo, S.; Jiang, Y. Absorption and EPR spectra of some porphyrins and metalloporphyrins. *Dyes Pigm.* **2007**, *74*, 357−362.
(43) Song, F.; Ma, P.; Chen, C.; Jia, J.; Wang, Y.; Zhu, P. Room temperature NO_2 sensor based on highly ordered porphyrin nanotubes. *J. Colloid Interface Sci.* **2016**, *474*, 51−57.
(44) Wang, Y.; Ma, P.; Song, F.; Yao, S.; Chen, C.; Zhu, P. Comparative NO_2-sensing in cobalt and metal-free porphyrin nanotubes. *J. Colloid Interface Sci.* **2017**, *490*, 129−136.
(45) Cho, B.; Lee, K.; Pyo, S.; Kim, J. Fabrication and characterization of VOC sensor array based on SnO_2 and ZnO nanoparticles functionalized by metalloporphyrins. *Micro Nano Syst. Lett.* **2018**, *6*, No. 10.
(46) Wang, Y.; Liu, D.; Yin, J.; Shang, Y.; Du, J.; Kang, Z.; Wang, R.; Chen, Y.; Sun, D.; Jiang, J. An ultrafast responsive NO_2 gas sensor based on a hydrogen-bonded organic framework material. *Chem. Commun.* **2020**, *56*, 703−706.
(47) Liu, Q.; Sun, Q.; Wei, C.; Li, X.; Yu, S.; Li, J.; Chen, Y. High-performance and wearable hazardous gases sensor based on n-n heterojunction film of NGO and tetrakis(1-pyrenyl)porphyrin. *J. Hazard. Mater.* **2021**, *419*, No. 126460.
(48) Zhu, P.; Li, S.; Jiang, Z.; Wang, Q.; Fan, F.; Yan, M.; Zhang, Y.; Zhao, P.; Yu, J. Noninvasive and wearable respiration sensor based on organic semiconductor film with strong electron affinity. *Anal. Chem.* **2019**, *91*, 10320−10327.
(49) Lee, J.-S.; Jeong, D.-W.; Byun, Y. T. Porphyrin nanofiber/single-walled carbon nanotube nanocomposite-based sensors for monitoring hydrogen peroxide vapor. *Sens. Actuators, B* **2020**, *306*, No. 127518.
(50) Zhu, P.; Li, S.; Zhao, C.; Zhang, Y.; Yu, J. 3D synergistical rGO/Eu(TPyP)(Pc) hybrid aerogel for high-performance NO_2 gas sensor with enhanced immunity to humidity. *J. Hazard. Mater.* **2020**, *384*, No. 121426.
(51) Zhu, P.; Wang, Y.; Ma, P.; Song, F.; Han, X.; Yao, S.; Yang, C. Highly ordered sandwich-type (phthalocyaninato) (porphyrinato) europium double-decker nanotubes and room temperature NO_2 sensitive properties. *Dalton Trans.* **2017**, *46*, 1531−1538.
(52) Sun, Q.; Liu, Q.; Gong, L.; Wang, C.; Kong, X.; Yang, C.; Feng, W.; Qi, D.; Dai, F.; Li, X.; Chen, Y. Hierarchical self-assembly of tetrakis(1-pyrenyl)porphyrins into microscopic petals and flowers with ultrasensitive room-temperature NO_2 sensing in a broad humidity range. *ChemNanoMat* **2019**, *5*, 1408−1417.
(53) Bengasi, G.; Meunier-Prest, R.; Baba, K.; Kumar, A.; Pellegrino, A. L.; Boscher, N. D.; Bouvet, M. Molecular engineering of porphyrin-tapes/phthalocyanine heterojunctions for a highly sensitive ammonia sensor. *Adv. Electron. Mater.* **2020**, *6*, No. 2000812.
(54) Figaro Engineering Inc. Products, Gas Sensors 2026 https://www.figaro.co.jp/en/product/docs/tgs2603_product%20information%28en%29_rev08.pdf. accessed on July 25th.
(55) Xu, L.; Li, T.; Wang, Y. A Novel Three-Dimensional Microheater. *IEEE Electron Device Lett.* **2011**, *32* (9), 1284−1286.
(56) Dai, Z.; Xu, L.; Duan, G.; Li, T.; Zhang, H.; Li, Y.; Wang, Y.; Wang, Y.; Cai, W. Fast-Response, Sensitivitive and Low-Powered Chemosensors by Fusing Nanostructured Porous Thin Film and IDEs-Microheater Chip. *Sci. Rep.* **2013**, *3*, No. 1669.
(57) Yan, Y.; Liu, J.; Liu, Q.; Yu, J.; Chen, R.; Zhang, H.; Song, D.; Yang, P.; Zhang, M.; Wang, J. Ag-modified hexagonal nanoflakes-textured hollow octahedron Zn_2SnO_4 with enhanced sensing properties for triethylamine. *J. Alloys Compd.* **2020**, *823*, No. 153724.
(58) Li, S.; Zhang, Y.; Han, L.; Li, X.; Xu, Y. Hierarchical kiwifruit-like ZnO/$ZnFe_2O_4$ heterostructure for high-sensitive triethylamine gaseous sensor. *Sens. Actuators, B* **2021**, *344*, No. 130251.
(59) Xu, X.; Wang, S.; Liu, W.; Chen, Y.; Ma, S.; Yun, P. An excellent triethylamine (TEA) sensor based on unique hierarchical MoS_2/ZnO composites composed of porous microspheres and nanosheets. *Sens. Actuators, B* **2021**, *333*, No. 129616.
(60) Fan, Y.; Xu, Y.; Wang, Y.; Sun, Y. Fabrication and characterization of Co-doped ZnO nanodiscs for selective TEA

Downloaded from pubs.acs.org/aanmf6/article-pdf/9/33/16061/6652075/acsanm.6c02958.pdf by guest on 22 October 2026

sensor applications with high response, high selectivity and ppb-level detection limit. *J. Alloys Compd.* **2021**, *876*, No. 160170.
(61) Yuan, Q.; He, L.; Zhang, K. Porous layered $ZnFe_2O_4$/ZnO heterostructure for enhanced triethylamine detection. *Mater. Sci. Semicond. Process.* **2024**, *176*, No. 108317.
(62) Liu, Z.; Wang, Y.; Li, Y.; Sui, C.; Liu, Y.; Liu, Y.; Zhao, Y.; Liang, X.; Liu, F.; Lu, G. Bimetallic MOF derived mesoporous structure of Ru doped SnO_2 enable high-sensitivity gas sensors for triethylamine in high humidity. *Sens. Actuators, B* **2024**, *405*, No. 135275.
(63) Shan, L.-X.; Li, Y.; Wang, R.-C.; Lian, X.-X. Sensing properties of ZnS@ZnO core-shell based triethylamine sensor fabricated using solvothermal and sintering methods. *J. Alloys Compd.* **2023**, *944*, No. 169223.
(64) Chernyadyev, A. Y.; Aleksandrov, A. E.; Lypenko, D. A.; Tyurin, V. S.; Tameev, A. R.; Tsivadze, A. Y. Copper(II) meso-Tetraphenyl- and meso-Tetrafluorenyl Porphyrinates as Charge Carrier Transporting and Electroluminescent Compounds. *ACS Omega* **2022**, *7* (10), 8613−8622.
(65) Pham, C. V.; Repp, S.; Thomann, R.; Krueger, M.; Weber, S.; Erdem, E. Charge transfer and surface defect healing within ZnO nanoparticle decorated graphene hybrid materials. *Nanoscale* **2016**, *8*, 9682−9687.
(66) Anju; Saini, L. K.; Pandey, M. Quantum chemical analysis of porphyrin-based sensors: Adsorption and sensing capabilities of pure, protonated, and metallic porphyrins insights into volatile organic compounds (VOCs). *Mater. Today Commun.* **2024**, *41*, No. 110989.
(67) Barsan, N.; Weimar, U. Conduction Model of Metal Oxide Gas Sensors. *J. Electroceram.* **2001**, *7*, 143−167.
(68) Magna, G.; Sivalingam, Y.; Martinelli, E.; Pomarico, G.; Basoli, F.; Paolesse, R.; Di Natale, C. The influence of film morphology and illumination conditions on the sensitivity of porphyrins-coated ZnO nanorods. *Anal. Chim. Acta* **2014**, *810*, 86−93.

Downloaded from pubs.acs.org/aanmf6/article-pdf/9/33/16061/6652097S/acsanm.6c02958.pdf by guest on 22 October 2026

https://doi.org/10.1021/acsanm.6c02958
ACS Appl. Nano Mater. 2026, 9, 16061−16074